International Journal of Research and Review
Volume 11; Issue: 11; November 2024
Website: www.ijrrjournal.com
Research Paper *E-ISSN: 2349-9788; P-ISSN: 2454-2237*

Enhanced Optoelectronic Properties of Few-Layer Graphene for Transparent Conducting Electrode: Density Functional Theory Perspective

Erik Bhekti Yutomo[1], Oki Ade Putra[2], Suci Faniandari[3], Dhani Nur Indra Syamputra[4], Muhammad Fahmi[5]

[1,2,3,4,5] Department of Physics, Faculty of Science and Mathematics, Diponegoro University, Semarang, 50275, Indonesia.

Corresponding Author: Erik Bhekti Yutomo

DOI: https://doi.org/10.52403/ijrr.20241109

ABSTRACT

The challenge in utilizing graphene for transparent conducting electrodes (TCE) is to increase the electronic conductivity without significantly decreasing its transmittance. Forming a few-layer structure is an effective way to modify the electronic properties of graphene. In this paper, we used the density functional theory (DFT) method to study the effect of the number of few-layer graphene (FLG) layers on the electronic conductivity and transmittance. We find that increasing the number of layers leads to an increase in electronic conductivity. On the other hand, a decrease in transmittance was observed when the number of layers was increased. Based on the performance analysis, the optoelectronic properties of FLG with more than three layers were better than those of conventional TCE materials, such as indium tin oxide (ITO) and aluminium-doped zinc oxide (AZO). The calculated electronic conductivity and transmittance of a 4-layer FLG were 2.23×10^{19} (1/Ω.m.s) and 95.69%, respectively. This finding can be used as guidance for experimental research in developing graphene-based TCE materials.

Keywords: density functional theory, electronic conductivity, few-layer graphene, transmittance

INTRODUCTION

Transparent conducting electrodes (TCE) are essential in today's electronic devices, such as solar cells, supercapacitors, touch screens, and flexible displays (1,2). In solar cells, for instance, TCE acts as a transparent layer, allowing sunlight to penetrate the active layer while conducting the resulting electric current (3,4). To obtain optimum performance, TCE materials must have excellent optoelectronic properties, such as high electronic conductivity and transmittance. However, both properties have an inverse relationship; for example, if we increase the electronic conductivity, the transmittance will decrease, and vice versa (5,6). Conventional TCE materials are still dominated by indium tin oxide (ITO) because it has high electronic conductivity and high transmittance (7,8). However, ITO as a TCE material has several drawbacks, namely high fabrication costs and mechanical properties unsuitable for flexible electronic devices (9). Therefore, finding alternative TCE materials outside ITO-based is one of the current focuses.

Graphene, a two-dimensional material with exceptional optoelectronic properties, including a high transmittance of 97%, can now be fabricated on an industrial scale using the modified (chemical vapour deposition) CVD method (10,11). This opens up exciting possibilities for its use as a TCE material. The application of graphene for TCE materials still faces several challenges, such as low electronic conductivity due to its two-dimensional structure (12,13). Several attempts have been made to improve the electronic conductivity of graphene, for example, by using doping techniques (14,15). However, doping techniques can make the graphene structure unstable due to chemical contamination. Recent progress shows that the formation of few-layer graphene (FLG) structures can improve electronic conductivity (16). However, this study has yet to be supported by in-depth computational studies.

On the other hand, the density functional theory (DFT) method has been widely used to study the optoelectronic properties of materials. The main advantage of the DFT method is that we can predict the properties of materials without doing direct experiments. DFT studies have succeeded in providing several findings in the development of TCE materials, such as obtaining the optimum concentration of aluminum (Al) atoms in aluminium-doped zinc oxide (AZO) thin film-based TCE materials (17,18). Based on these achievements, we would like to use the DFT method to study the optoelectronic properties of FLG. We have found that increasing the number of layers can increase the conductivity but decrease the transmittance. Based on the performance analysis, we found that FLG with more than three layers has a good combination of conductivity and transmittance, so its performance is higher than ITO and AZO.

COMPUTATIONAL METHODOLOGY

This study modeled FLG with AB stacking because it has good structural stability and is often obtained during graphene growth (19,20). An illustration of the crystal structure of FLG can be seen in Figure 1. In this study, we varied the FLG layers from 1 to 5. An isolated model was constructed by applying a vacuum system of 10 Å to avoid nearest-neighbor interactions. All electronic, optical, and transport properties calculations were performed using density functional theory (DFT) methods implemented in the Quantum ESPRESSO code (21,22). The projector augmented-wave (PAW) type pseudopotential and the generalized gradient approximation (GGA) type exchange-correlation functional based on Perdew–Burke–Ernzerhof (PBE) were chosen to simplify the interaction of electrons with the nucleus and approximate the interaction between valence electrons, respectively (23,24). This pseudopotential only considers the 2s and 2p electron configurations of the C atom. To obtain high accuracy and reasonable simulation time in the geometry optimization and SCF calculation, the k-point, cut-off energy, energy threshold, and force threshold were set to 7×7×1, 816 eV, 13.6 meV, and 25 meV/Å, respectively. In PDOS and transport properties calculations, the k-points were enlarged 10-fold to 70×70×1 to dense the k-points and thus improve accuracy. Before performing optical, and transport properties calculations, the lattice parameters and atomic positions of each system were optimized using the Broyden–Fletcher–Goldfarb–Shanno (BFGS) method (25–28).

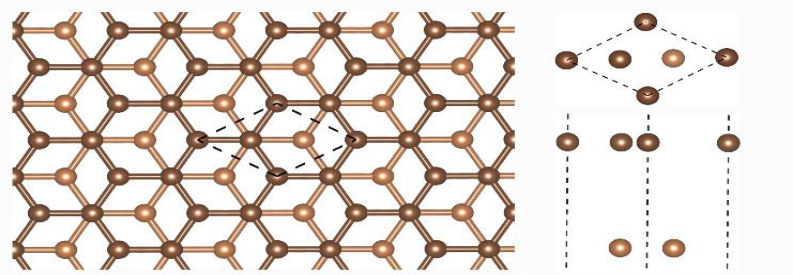

Figure 1. The Crystal structure of few-layer graphene (FLG) with AB stacking. The black dashed line indicates the unit cell used in the DFT calculations.

The calculation of optical properties begins with the complex dielectric function (ε_1+iε_2). The imaginary part of the dielectric function (ε_2) was obtained using the Drude-Lorentz model, while the real part of the dielectric function (ε_1) was obtained using the Kramers-Kronig relation. Both are expressed by the equation 1 and 2, respectively.

$$\varepsilon_1(\omega) = 1 + \frac{2}{\pi} P \int_0^\infty \frac{\varepsilon_2(\omega')\,\omega'}{\omega'^2 - \omega^2} d\omega' \quad (1)$$

and,

$$\varepsilon_2(\omega) = -\frac{2\omega}{\pi} P \int_0^\infty \frac{[\varepsilon_1(\omega') - 1]}{\omega'^2 - \omega^2} d\omega' \quad (2)$$

where,

$$P\int_0^\infty d\omega' = \lim_{\delta\to 0}\left(\int_0^{\omega-\delta} d\omega' + \int_{\omega-\delta}^\infty d\omega'\right) \quad (3)$$

From the complex dielectric function, we can determine the complex refractive index (n+ik) using equation 4 and 5, respectively.

$$n(\omega) = \left(\frac{1}{\sqrt{2}}\right)\left[\sqrt{\varepsilon_1(\omega)^2 + \varepsilon_2(\omega)^2} + \varepsilon_1(\omega)\right]^{1/2} \quad (4)$$

and,

$$k(\omega) = \left(\frac{1}{\sqrt{2}}\right)\left[\sqrt{\varepsilon_1(\omega)^2 + \varepsilon_2(\omega)^2} - \varepsilon_1(\omega)\right]^{1/2} \quad (5)$$

From complex refractive index, the important parameters of optical properties can be determined, including reflectance (R(ω)), transmittance (T(ω)), and absorption coefficient (α(ω)) using the equations 6,7, and 8, respectively.

$$R(\omega) = \frac{[1 - n(\omega)]^2 + k(\omega)^2}{[1 + n(\omega)]^2 + k(\omega)^2} \quad (6)$$

$$\alpha(\omega) = 2\omega\, k(\omega) \quad (7)$$

and,

$$T(\omega) = (1 - R)^2\, e^{-\alpha d} \quad (8)$$

where d is the layer thickness.

The transport properties were analyzed by calculating the electronic conductivity using the Boltzmann transport theory and the constant relaxation time approximation. The electronic conductivity can be calculated by the equation 9.

$$\sigma = e^2 \mathcal{L}_0 \quad (9)$$

where e is the electron charge and $\mathcal{L}_0$ is the 0th order thermoelectric integral related to the transport distribution function which can be formulated by the equation 10.

$$\mathcal{L}_0 = \int \tau v^2 \, g(E) \left(-\frac{\partial f}{\partial E}\right) dE \quad (10)$$

where g(E) is the DOS and τ is the relaxation time constant. The integration is performed numerically by considering the energy dispersion E as a function of the discrete electron wave vectors from the DFT calculation.

RESULT AND DISCUSSION

First, we evaluate the structural properties of FLG to check the accuracy of the simulation parameters. Table 1 summarizes the calculation results of several important structural properties, such as the lattice constant (a), interlayer spacing (d_{int}), and bond length between C atoms ($d_{\text{C-C}}$). The lattice constant and the bond length between C atoms of FLG 1L (single-layer graphene) agree with the structural properties observed in experimental studies (29,30). Moreover, the lattice constant, the interlayer distance, and the bond length between C atoms of the FLG 2L (bilayer graphene) are consistent with previous computational studies (31). This condition indicates that the calculation parameters used in this study are appropriate. Furthermore, increasing the number of layers causes the interlayer spacing to decrease. In FLG 5L, the interlayer spacing approaches the distance between layers in graphite, which is 3.34 Å. This result is acceptable because increasing the number of layers causes the Coulomb interaction between layers to be stronger, causing the interlayer spacing to decrease.

Table 1. The calculation results of the lattice constant (a), the interlayer spacing (d_{int}), and the bond length between C atoms ($d_{\text{C-C}}$)

FLG	a (Å)	d_{int} (Å)	$d_{\text{C-C}}$ (Å)
1 layer (1L)	2.465	-	1.423
2 layers (2L)	2.464	3.512	1.423
3 layers (3L)	2.463	3.511	1.422
4 layers (4L)	2.463	3.511	1.422
5 layers (5L)	2.462	3.337	1.421

The analysis of optical properties begins with calculating the complex dielectric function ($\varepsilon_1+i\varepsilon_2$) dependent on the field polarization direction. The field polarization direction is set relative to the c-axis, where E⊥c indicates the field polarization perpendicular to the c-axis, while E∥c indicates the field polarization parallel to the c-axis. Figure 2(a) shows the real part of the dielectric function (ε_1) of FLG 1L. The static dielectric constant has a finite value of 1.67 for E∥c. This characteristic is in good agreement with that reported by several previous computational studies (32,33). Figure 2(b) shows the imaginary part of the dielectric function of FLG 1L. The imaginary part contains information on absorption peaks related to interband transitions for the high-energy region and intraband transitions for the low-energy region. For the case of E⊥c, there are two absorption peaks, namely at 3.9 eV related to the π→π* transition and at 13.78 eV related to the σ→σ* transition. Furthermore, there are two significant absorption peaks at 10.69 eV corresponding to the π→σ* transition and at 13.19 eV corresponding to the σ→π* transition for E∥c. The characteristics of the imaginary part obtained in this study are consistent with those of previous computational studies (32,33). Figure 2 (c) shows the electronic band structure of FLG 1L and its electronic transitions to help understand the allowed electronic transitions.

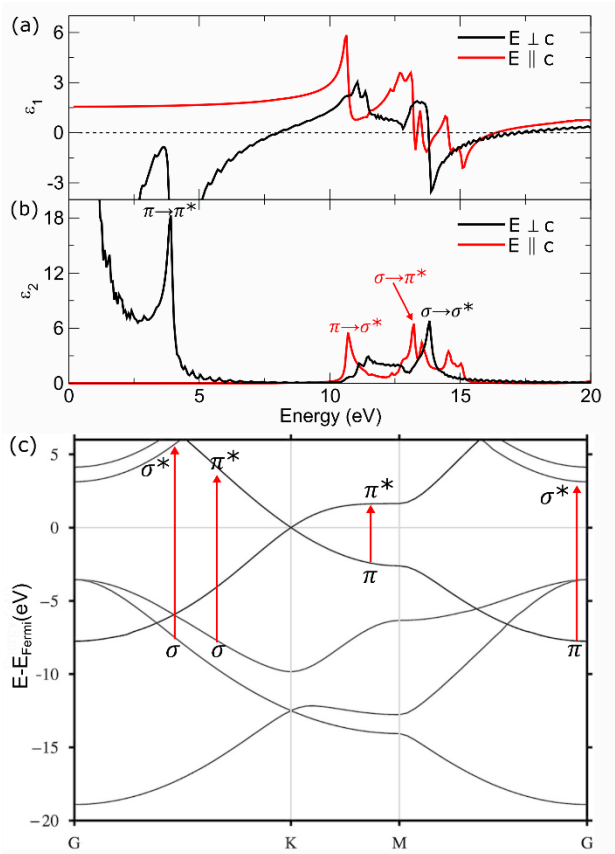

Figure 2. The complex dielectric function of the FLG 1L (ε_1+iε_2) (a) for the real part (ε_1) and (b) for the imaginary part (ε_2). (c) The electronic band structure of the FLG 1L with allowed electronic transitions.

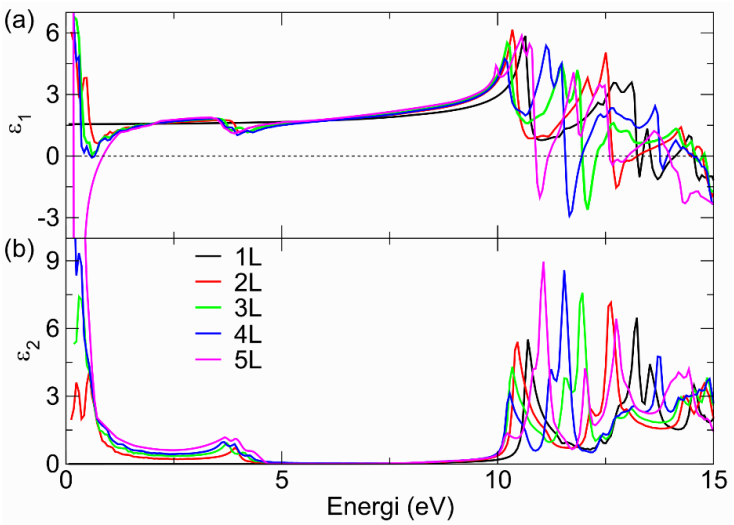

Figure 3. The complex dielectric function (ε_1+iε_2) for the E∥c case of FLG with various numbers of layers (a) for the real part (ε_1) and (b) for the imaginary part (ε_2).

To analyze the effect of the number of layers, we only consider the complex dielectric function for the case of E∥c. Increasing the number of layers causes the real dielectric function (ε_1) to diverge at low energy, as shown in Figure 3(a). This condition is related to the transformation of the electronic properties of FLG into metal when the number of layers is increased. Interestingly, increasing the number of layers causes an increase in the ε_1 intensity over a wide energy range of 1.9 eV to 3.6 eV. This energy range covers part of the ultraviolet (UV) region and the visible light (VL) region. For the imaginary part (ε_2), increasing the number of layers

gives rise to a high absorption peak in the low-energy region, as shown in Figure 3(b). This peak is related to the new intraband transition due to the addition of layers.

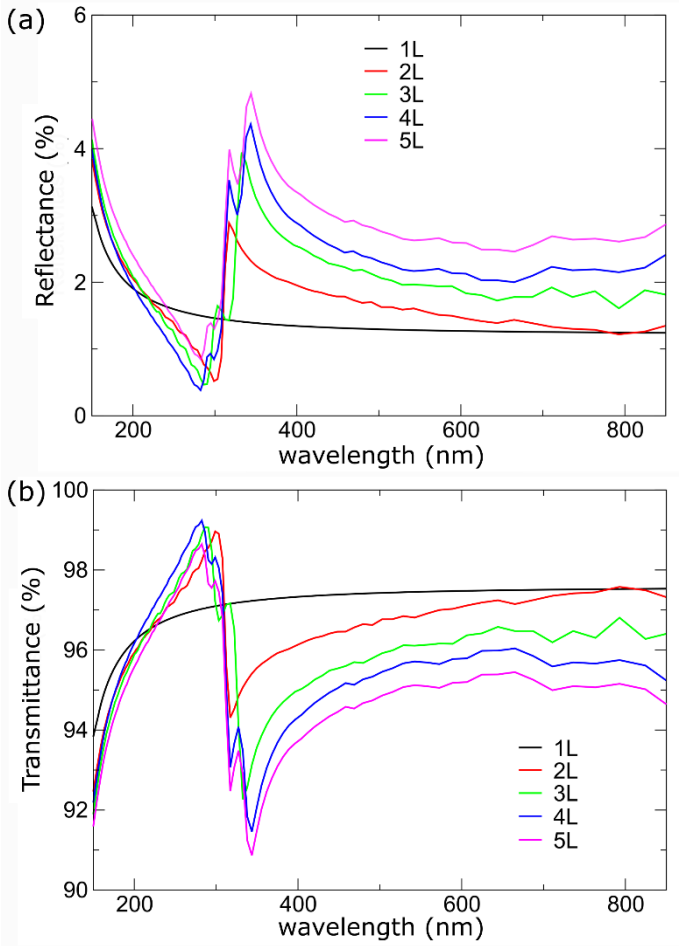

Figure 4. (a) Reflectance and (b) transmittance of the FLG with various layers.

From the complex dielectric function, we can calculate the reflectance and transmittance of FLG using Equations 6 and 8, respectively. Reflectance and transmittance are crucial parameters in TCE applications. The reflectance and transmittance as a function of wavelength are shown in Figure 4(a) and (b), respectively. We consider the wavelength range of 150-850 nm, which covers part of the UV and infrared (IR) regions and the entire VL region. FLG 1L has a reflectance of 1.4% and a transmittance of 97.5% in the VL region. These results are consistent with experimental facts, where SLG has transparent properties with a transmittance of 97% (11). In the UV region, FLG 1L experiences a decrease in transmittance related to the dominant absorption in the UV region, as shown in the analysis of the imaginary part of the dielectric function.

Increasing the number of graphene layers causes an increase in reflectance and a decrease in transmittance in the VL and near-IR regions. This result is acceptable because increasing the number of layers means increasing the thickness of the FLG. Thus, the possibility of electromagnetic waves being absorbed or refracted by the FLG is higher. This fact is supported by the imaginary dielectric function analysis results, which show an increase in intensity in the energy range of 1.9 eV to 3.6 eV, as shown in Figure 3(b). The increase in intensity of the imaginary dielectric function is related to the increase in electromagnetic wave absorption for electronic transitions.

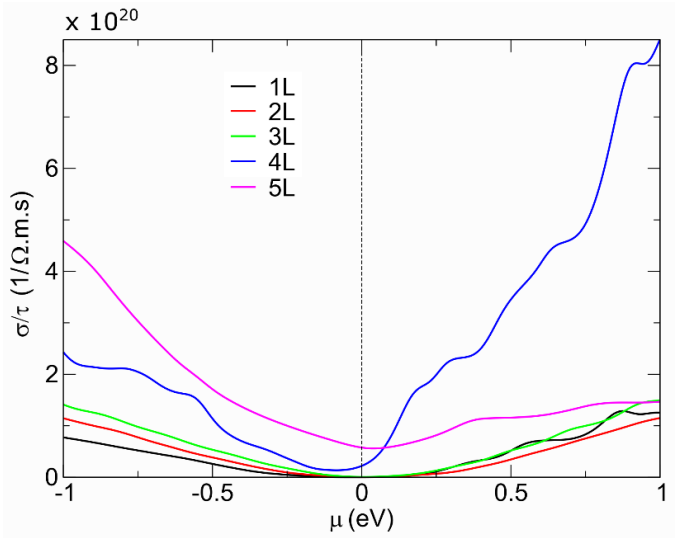

Figure 5. The electronic conductivity of FLG with various number of layers.

Transport properties analysis was performed by calculating the electronic conductivity (σ) using Equation 9. Electronic conductivity is also one of the crucial parameters in the development of TCE materials. Figure 5 shows the calculated electronic conductivity. First, we focus on intrinsic conductivity, which is the conductivity when the chemical potential (μ) is zero. FLG 1L, 2L, 3L, 4L, and 5L have intrinsic conductivities of 1.03×10^{17}, 2.34×10^{17}, 6.64×10^{17}, 2.23×10^{19}, dan 5.77×10^{19} $(\Omega.m.s)^{-1}$, respectively. These results clearly show that forming FLG structures can enhance the electronic conductivity of graphene. The increase in electronic conductivity is related to the transformation of the electronic properties of graphene from semi-metallic to metallic when the number of layers is increased. Further optimization of electronic conductivity can be done by doping either p-type or n-type doping. Doping can increase the electronic conductivity of graphene two-fold, as shown in Figure 5. Several experimental studies have also reported that doping techniques can be used to improve the conductivity of graphene (34–36). In this study, the optimum conductivity was obtained when FLG 4L was doped with n-type.

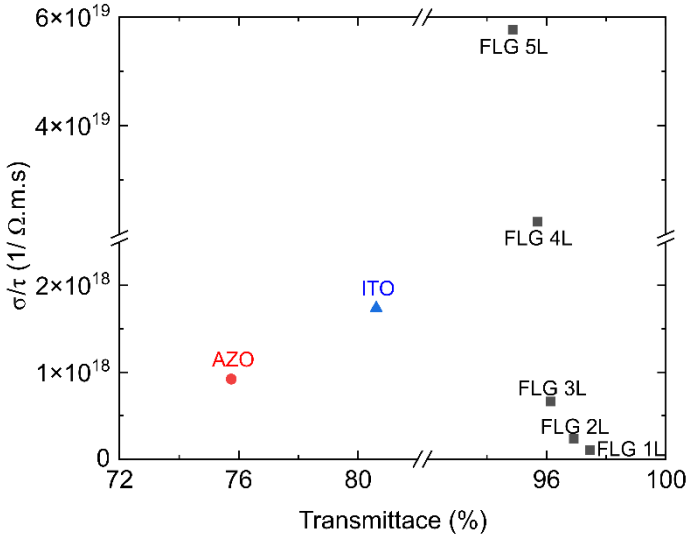

Figure 6. Transmittance versus electronic conductivity of the FLG with various number of layers and the conventional TCE materials (AZO and ITO)

We plotted the transmittance versus electronic conductivity to compare the performance of FLG-based and conventional TCEs, as shown in Figure 6. We only considered the transmittance at 550 nm wavelength and the intrinsic electronic conductivity. The AZO and ITO were modeled using a thin film of four isolated layers with a vacuum space of 10 Å. The concentrations of Al and In were set at 16.67%. Based on previous studies, this composition can produce optimum performance of AZO and ITO in TCE applications (37). Figure 6 shows that the FLG always has a higher transmittance than AZO or ITO, even for FLG 5L. ITO has a transmittance of 82.61%, consistent with the experimental results of ~80% (38). Besides transmittance, electronic conductivity is also a crucial factor in TCE performance. The electronic conductivity of FLG with less than four layers is smaller than ITO and comparable to AZO. On the other hand, FLG with more than three layers has significantly higher conductivity than ITO and AZO. Therefore, we predict that FLG with more than three layers has better performance than conventional TCE materials.

CONCLUSION

We have studied the effect of the number of layers on the electronic conductivity and transmittance of FLG. The variation of the number of layers is 1-5 layers. We validate the simulation parameters by comparing the calculated structural properties with previous computational studies and experimental results. Increasing the number of FLG layers increases the intensity of the imaginary dielectric function in the low-energy region, indicating the enhancement of ultraviolet and visible light absorption by FLG. This condition causes a decrease in transmittance when the number of FLG layers increases. Furthermore, increasing the number of FLG layers causes the transformation of electronic properties from semimetal to metal, resulting in an increase in electronic conductivity. Electronic conductivity can be further enhanced by providing n-type or p-type doping. Finally, we find that FLG with more than three layers has better performance than conventional TCE materials, such as ITO and AZO.

Declaration by Authors

Acknowledgement: None
Source of Funding: None
Conflict of Interest: The authors declare no conflict of interest.

REFERENCES

1. Nguyen VH, Papanastasiou DT, Resende J, Bardet L, Sannicolo T, Jiménez C, et al. Advances in Flexible Metallic Transparent Electrodes. Small. 2022; 18(19):2106006.
2. Wan J, Xia Y, Fang J, Zhang Z, Xu B, Wang J, et al. Solution-Processed Transparent Conducting Electrodes for Flexible Organic Solar Cells with 16.61% Efficiency. Nano-Micro Letters 2021; 13(1):44.
3. Koo D, Jung S, Seo J, Jeong G, Choi Y, Lee J, et al. Flexible Organic Solar Cells Over 15% Efficiency with Polyimide-Integrated Graphene Electrodes. Joule. 2020; 4(5):1021–34.
4. Gao ZW, Wang Y, Liu H, Sun J, Kim J, Li Y, et al. Tailoring the Interface in $FAPbI_3$ Planar Perovskite Solar Cells by Imidazole-Graphene-Quantum-Dots. Advanced Functional Materials. 2021; 31(27):2101438.
5. Du J, Zhang D, Wang X, Jin H, Zhang W, Tong B, et al. Extremely efficient flexible organic solar cells with a graphene transparent anode: Dependence on number of layers and doping of graphene. Carbon. 2021; 171:350–8.
6. Sahu RS, Li DL, Doong R an. Unveiling the hydrodechlorination of trichloroethylene by reduced graphene oxide supported bimetallic Fe/Ni nanoparticles. Chemical Engineering Journal. 2018; 334:30–40.
7. Singh R, Tharion J, Murugan S, Kumar A. ITO-Free Solution-Processed Flexible Electrochromic Devices Based on PEDOT: PSS as Transparent Conducting Electrode. ACS Applied Materials & Interfaces. 2017; 9(23):19427–35.

8. Ali AH, Abu Bakar AS, Hassan Z. Improved optoelectronics properties of ITO-based transparent conductive electrodes with the insertion of Ag/Ni under-layer. Applied Surface Science. 2014; 315:387–91.
9. Lee HB, Jin WY, Ovhal MM, Kumar N, Kang JW. Flexible transparent conducting electrodes based on metal meshes for organic optoelectronic device applications: a review. Journal of Materials Chemistry C. 2019; 7(5):1087–110.
10. Zhu Y, Ji H, Cheng HM, Ruoff RS. Mass production and industrial applications of graphene materials. National Science Review. 2018; 5(1):90–101.
11. Bonaccorso F, Sun Z, Hasan T, Ferrari AC. Graphene photonics and optoelectronics. Nature Photonics. 2010; 4(9):611–22.
12. Peng Y, Liu Z, Tai Q, Liu S, Yan F. Efficient Semitransparent Perovskite Solar Cells with Graphene Electrodes. Advanced Materials. 2015; 27(24):3632-3638.
13. Choi YY, Kang SJ, Kim HK, Choi WM, Na SI. Multilayer graphene films as transparent electrodes for organic photovoltaic devices. Solar Energy Materials and Solar Cells. 2012; 96:281–5.
14. Kim S, Shin SH, Choi SH. N-i-p-type perovskite solar cells employing n-type graphene transparent conductive electrodes. Journal of Alloys and Compounds. 2019; 786:614–20.
15. Patel K, Tyagi PK. P-type multilayer graphene as a highly efficient transparent conducting electrode in silicon heterojunction solar cells. Carbon. 2017; 116:744–52.
16. Lancellotti L, Bobeico E, Della Noce M, Mercaldo LV, Usatii I, Delli Veneri P, et al. Graphene as non conventional transparent conductive electrode in silicon heterojunction solar cells. Applied Surface Science. 2020; 525:146443.
17. Wu M, Sun D, Tan C, Tian X, Huang Y. Al-Doped ZnO Monolayer as a Promising Transparent Electrode Material: A First-Principles Study. Materials. 2017; 10(4):359.
18. Saxena N, Manzhi P, Choudhary RJ, Upadhyay S, Ojha S, Umapathy GR, et al. Performance optimization of transparent and conductive $Zn_{1-x}Al_xO$ thin films for opto-electronic devices: An experimental & first-principles investigation. Vacuum. 2020; 177:109369.
19. Liu L, Zhou H, Cheng R, Yu WJ, Liu Y, Chen Y, et al. High-Yield Chemical Vapor Deposition Growth of High-Quality Large-Area AB-Stacked Bilayer Graphene. ACS Nano. 2012; 6(9):8241–9.
20. Yang G, Li L, Lee WB, Ng MC. Structure of graphene and its disorders: a review. Science and Technology of Advanced Materials. 2018; 19(1):613–48.
21. Giannozzi P, Andreussi O, Brumme T, Bunau O, Nardelli MB, Calandra M, et al. Advanced capabilities for materials modelling with Quantum ESPRESSO. Journal of Physics: Condensed Matter. 2017; 29(46):465901.
22. Giannozzi P, Baroni S, Bonini N, Calandra M, Car R, Cavazzoni C, et al. QUANTUM ESPRESSO: a modular and open-source software project for quantum simulations of materials. Journal of Physics: Condensed Matter. 2009; 21(39):395502.
23. Blöchl PE. Projector augmented-wave method. Physical Review B. 1994; 50(24):17953–79.
24. Perdew JP, Burke K, Ernzerhof M. Generalized Gradient Approximation Made Simple. Physical Review Lett. 1996; 77(18):3865–8.
25. Broyden CG. The Convergence of a Class of Double-rank Minimization Algorithms 1. General Considerations. IMA Journal of Applied Mathematics. 1970; 6(1):76–90.
26. Fletcher R. A new approach to variable metric algorithms. The Computer Journal. 1970; 13(3):317–22.
27. Shanno DF. Conditioning of quasi-Newton methods for function minimization. Mathematics of Computation. 1970 ;24(111):647–56.
28. Goldfarb D. A family of variable-metric methods derived by variational means. Mathematics of Computation. 1970; 24(109):23–6.
29. Xuesong Li, Weiwei Cai, Luigi Colombo, Rodney S. Ruoff. Evolution of Graphene Growth on Ni and Cu by Carbon Isotope Labeling. Nano Letter. 2009; 9(12):4268–72.
30. Li X, Cai W, An J, Kim S, Nah J, Yang D, et al. Large-Area Synthesis of High-Quality and Uniform Graphene Films on Copper Foils. Science. 2009; 324(5932):1312–4.
31. Wang Tao, Guo Qing, Liu Yan, Sheng Kuang. A comparative investigation of an AB- and AA-stacked bilayer graphene sheet under an applied electric field: A density functional theory study. Chinese Physics B. 2012; 21(6):067301.

32. Rani P, Dubey GS, Jindal VK. DFT study of optical properties of pure and doped graphene. Physica E: Low-dimensional Systems and Nanostructures. 2014; 62:28–35.
33. Sedelnikova OV, Bulusheva LG, Okotrub AV. Ab initio study of dielectric response of rippled graphene. The Journal of Chemical Physics. 2011; 134(24):244707.
34. Bian H, Wang Q, Yang S, Yan C, Wang H, Liang L, et al. Nitrogen-doped graphene quantum dots for 80% photoluminescence quantum yield for inorganic γ-$CsPbI_3$ perovskite solar cells with efficiency beyond 16%. Journal of Materials Chemistry A. 2019; 7(10):5740–7.
35. Bianco GV, Sacchetti A, Milella A, Grande M, D'Orazio A, Capezzuto P, et al. Extraordinary low sheet resistance of CVD graphene by thionyl chloride chemical doping. Carbon. 2020; 170:75–84.
36. Seo YM, Jang W, Gu T, Whang D. Highly Efficient n-Type Doping of Graphene by Vacuum Annealed Amine-Rich Macromolecules. Materials. 2020; 13(9):2166.
37. Hamberg I, Granqvist CG. Evaporated Sn-doped In2O3 films: Basic optical properties and applications to energy-efficient windows. Journal of Applied Physics. 1986: 60(11):R123–60.
38. Minami T. Transparent conducting oxide semiconductors for transparent electrodes. Semiconductor Science and Technology. 2005; 20(4): S35.

How to cite this article: Erik Bhekti Yutomo, Oki Ade Putra, Suci Faniandari, Dhani Nur Indra Syamputra, Muhammad Fahmi. Enhanced optoelectronic properties of few-layer graphene for transparent conducting electrode: density functional theory perspective. *International Journal of Research and Review*. 2024; 11(11): 69-78. DOI: *https://doi.org/10.52403/ijrr.20241109*

******